

# Mechanical properties of zinc oxide thin films grown by spray-pyrolysis

E. A. Villegas, R. Parra, L. A. Ramajo<sup>†</sup>

<sup>†</sup>lramajo@fimdp.edu.ar

Institute of Materials Science and Technology Research (INTEMA), National University of Mar del Plata (UNMdP), National Research Council of Argentina (CONICET), Mar del Plata, B7608FDQ, Argentina

Zinc oxide (ZnO) thin films are considered promising materials for optoelectronic applications, and characterization of their optical, electrical, and mechanical properties is essential for such purposes. In this study, thin films were deposited on glass substrates using spray-pyrolysis at 450°C, with film thicknesses ranging from 57 to 160 µm achieved by controlling the volume of the sprayed solution. ZnO thin films were characterized by XRD, where texture coefficient analysis was carried out to determine the preferential crystal growth, showing variations on (002), (100), (101) planes as the thickness of the film increases. The surface topography and grain size distribution of the films were analyzed using FE-SEM. The optical transmittance and optical bandgap of the thin films were studied by UV-Vis spectroscopy, with no significant change in the optical bandgap observed with varying thickness. Electrical properties were studied under the Van der Pauw method, obtaining conductivity values between 3.45 and 23.8 S. Finally, elastic modulus and film hardness were analyzed by instrumental indentation and calculated through the Hertz model, obtaining hardness and elastic modulus values between 4.5–6 GPa and 96.7–111.5 GPa, respectively. The observed increase in hardness was attributed to the densification around the indentation zone.

**Keywords:** zinc oxide, mechanical properties, thin films, spray pyrolysis.

## 1. Introduction

The study of the functional properties of ZnO thin films have shown their high transparency in the visible range of the electromagnetic spectrum [1]. In addition, conductivity in the order of semiconductors can be improved using doping agents [2, 3]. This set of qualities of ZnO-based thin films shows us that thin films can be used as transparent electrodes for solar cells and other optoelectronic devices [4, 5].

To achieve a good performance for these applications, and because of susceptibility to contact damage, ZnO-based films must present appropriate mechanical properties: hardness and resistance to scratching. Nanoindentation has been widely used to determine the elastic modulus and hardness of thin (ceramic) films [7–11]. Compared to the micro-indentation technique, nanoindentation does not require a separate measurement of the contacted area. The penetration depth of the specimen during nanoindentation is related to the actual contact area via a well-calibrated indenter tip. Then this technique offers a reliable approach to characterize the mechanical features of ultra-thin films, which is difficult to accomplish by other methods. A aspherical indenter is preferred to a sharp indenter (Berkovich), because even with a shallow indentation depth, the volume of material that is sufficiently large to include a large number of ceramic grains, can be assessed [6].

There are several parameters to take into account, apart from the electrical, optical and mechanical properties, to determine the criteria for the viability of thin films as

transparent electrodes according to Gordon [12]. In this work only the properties mentioned above have been studied. To determine the relationship between the thickness of thin films and hardness, it is necessary to make use of some models that explain the influence of indentation on the hardness of the material [13].

Although the mechanical properties of sprayed ceramic films have been rarely reported, there are interesting works focused on the behavior of ZnO films grown under different conditions [14–16]. In this paper, the effects of thickness and microstructure on the mechanical properties of ZnO thin films deposited by spray-pyrolysis on glass substrates at 450°C were studied. In the subsequent sections, these properties will be presented and discussed specifically for thin transparent films grown through the spraying method. The observed increase in hardness will be attributed to the densification that occurs around the indentation zone.

## 2. Experimental procedure

Zinc acetate (4 g,  $\text{Zn}(\text{OCOCH}_3)_2 \cdot 2\text{H}_2\text{O}$ , 98%) was dissolved in 40 ml of absolute ethanol (99.5%), under stirring, with the aid of small volumes of acetylacetone (99%). The resulting solution was sprayed through the nozzle of an airbrush onto  $\text{SiO}_2$ -coated glass substrates at 450°C with nitrogen as carrier gas at 2 bar. The distance between nozzle and substrate was kept at 15 cm throughout the procedure. Three films with different characteristics were prepared by spraying increasing volumes of the zinc acetate solution (50, 60, 70 ml).

The films were analyzed by means of grazing incidence-X-ray diffraction (GI-XRD) at 0.5° in a PANalytical X'Pert diffractometer. The texturing coefficient  $TC_{(hkl)}$  was calculated according to the Mueller equation as described elsewhere [18]. The microstructure of the films was also assessed by high resolution scanning electron microscopy (FE-SEM) in a FEI Quanta 250 FEG microscope, and the thicknesses were measured with a KLA Tecnor E-100 mechanical profilometer.

The mechanical properties as elastic modulus ( $E$ ) and hardness ( $H$ ) were determined by means of a Hysitron triboindenter. A Berkovich diamond indenter was used to measure 15 load-unload cycles with a 450  $\mu$ N load. A specific software was used to analyze the data sets and to build load-displacement curves [19], whereas the reduced modulus ( $E_r$ ) and the hardness of the films were determined by the Hertzian method [20, 21], which consists in the calculation of the slope of the unloading curve by first fitting the entire unloading data. It is possible to calculate the reduced elastic modulus, which is related to the elastic modulus and the contact stiffness ( $S$ ) according to equations (1)–(4).

$$P = ah^{3/2}, \quad (1)$$

$$a = \left( \frac{4}{3} E_r \sqrt{R} \right), \quad (2)$$

$$\frac{1}{E_r} = \frac{(1 - v^2)}{E} + \frac{(1 - v_i^2)}{E_i}, \quad (3)$$

$$E_r = S \left( \frac{\pi}{4A_{max}} \right)^{1/2}, \quad (4)$$

where  $v$  is the Poisson's ratio and subscript  $i$  denotes the indenter material,  $R$  represents the indenter radius of 25 nm,  $h$  is the displacement, and  $P$  is the applied force and  $A_{max}$  is the surface contact area at the maximum displacement. By fitting  $P-h$  curves,  $E_r$  is obtained. The contact stiffness ( $S$ ) was assumed as the slope of the unloading curve and taken as the first derivative in the maximum depth of a fitted power-law function of the unloading segment of the curve. For the indenter tip used in this work,  $E_i$  is 1140 GPa, and  $n_i$  is 0.07, while the Poisson ratio was taken as 0.25. The maximum load,  $P_{max}$ , which was defined dividing by the projected area of the indentation under this load, was used to find the material hardness  $H$ . A fused silica sample of known  $E$  was used to calibrate the tip area function  $A(hc)$ .

### 3. Results and discussion

The thickness of the films increases with the sprayed volume, as revealed by profilometry. Thickness values of 0.57, 1.25 and 1.6  $\mu$ m were measured for films Z5, Z12, and Z16, respectively. Films were also observed under FE-SEM magnification to assess the microstructure and determine grain morphology. Figure 1 shows surface images dominated by grains with elongated morphologies and apparently rough surfaces, which is similar to what has been reported by other researchers in systems obtained by spray pyrolysis [22]. The average grain sizes shown in Table 1 were obtained from the FE-SEM images for each film.

Figures 2 a and b show the XRD patterns and the texture coefficients (TC) calculated for the different ZnO films, respectively. The former confirms that films are single-phase ZnO, with diffraction peaks assigned to the wurtzite structure according to the JCPDS file 36-1451. In addition, some differences in relative intensities of specific peaks concerning the mentioned file are observed in Fig. 2 a. The thinnest film Z5 shows a high intensity (002) peak with respect to films Z12 and Z16 consistent with the preferential growth in the  $c$ -direction, whereas thicker samples (Z12 and Z16) show enhanced anisotropic crystal growth in the  $a$  and  $b$ -directions, perpendicular to the [001] direction. Accordingly, Fig. 2 b plots texture coefficients for the (002), (101), and (100) peaks as a function of sprayed volume and film thickness. It can be seen that  $TC_{(002)}$  is equal to 1.4 for Z5, implying a high  $c$ -orientation. Moreover, it appears that the greater the thickness, the smaller the  $TC_{(002)}$  value, or that the increase in thickness inhibits the growth along the [001] direction. The higher values of  $TC_{(101)}$  and  $TC_{(100)}$  imply that the  $c$ -orientation growth is inhibited and that crystals growth, preferentially, in the orthogonal [101] and [102] directions.

The optical transmittance spectra of the zinc oxide films are shown in Fig. 3. Average transmittance in the visible region (390–750 nm) of 78% was obtained for film Z5. However, a

**Table 1.** Thickness ( $t$ ), average grain size ( $d$ ), sheet resistance ( $R_{sh}$ ) and conductivity ( $S$ ).

Film	$t$ / mm	$d$ / nm	$R_{sh}$ / k $\Omega$ ·sq $^{-1}$	$S$ / ( $\Omega$ ·cm) $^{-1}$
Z5	5.7	120	5.10	3.45
Z12	1.25	225	0.46	17.3
Z16	1.60	320	0.26	23.8

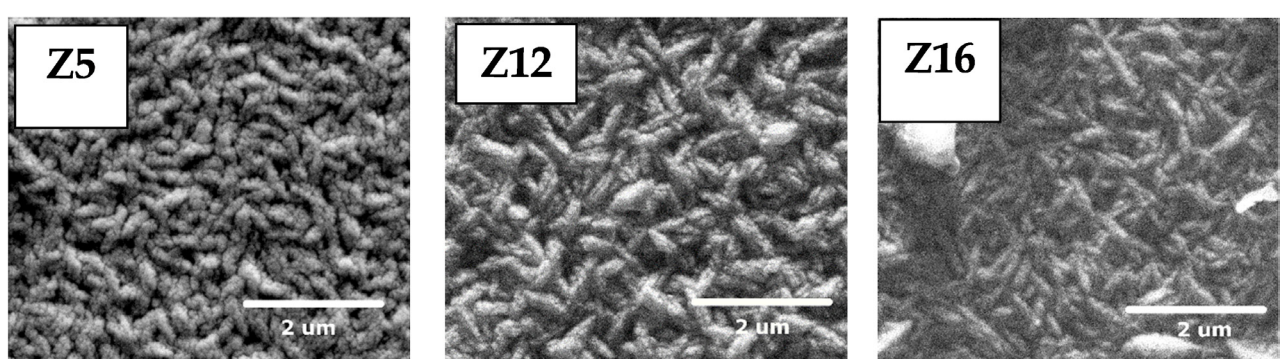


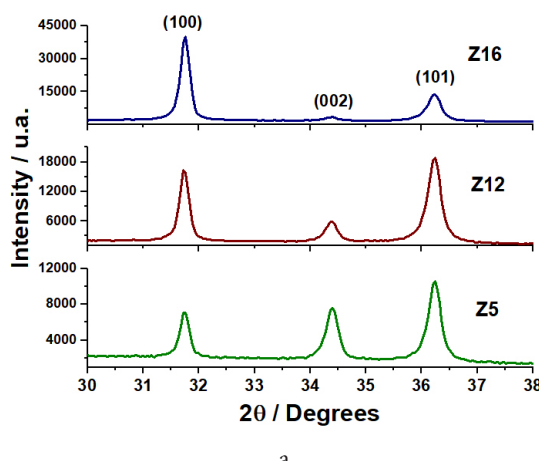
**Fig. 1.** FE-SEM images of ZnO films grown by spray-pyrolysis on glass substrates (scale bar 2  $\mu$ m).

decrease in transmittance is observed as the thickness of the films increases. The average visible transmittances for films Z12 and Z16 are of 75 and 73%, respectively. The bandgap energy of 3.2 eV, approximately, was estimated for every film from Tauc plots following a method described previously [2]. In order to fully characterize the prepared films and to allow comparisons with similar films, the sheet resistance was measured and the conductivity calculated. The results shown in Table 1 indicate, as expected, that conductivity increases with grain size.

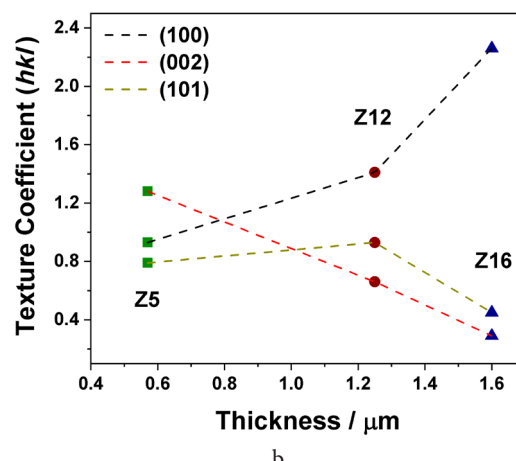
Figure 4 shows load-displacement curves for ZnO films with different thicknesses (Z5, Z12, and Z16). From the parameter  $a$  of Eq. (2), the apparent elastic modulus is calculated, for which the graphs were fitted using polynomial curves with power 3/2 to fit with the Hertzian model. Because

measurements were made under displacement control setting in order to comply with the 5% rule and to avoid the influence of the substrate, the maximum load increases with film thickness. The maximum load applied increases from film Z5 to film Z16 leading to a gradual increase in apparent hardness  $H$ , as shown in Table 2. As suggested in the literature, when porous ceramic films are assessed, the collapse and densification of the microstructure under the indenter must be considered [26].

The ZnO films are single phase with grain sizes ranging 120–320 nm. The grain boundaries act as strain compensation sites responsible for the absence of pop-in events [25]. Zhao discusses the enhancement of the hardness of ZnO thin films at different thicknesses and microstructures [27]. In simple



a



b

**Fig. 2.** (Color online) XRD patterns (a) and texture coefficients corresponding to the main diffraction planes of ZnO films with different thicknesses (b).

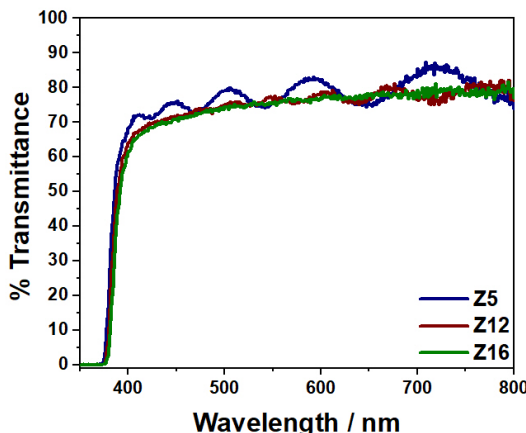


**Fig. 3.** (Color online) Optical transmittance of ZnO films.

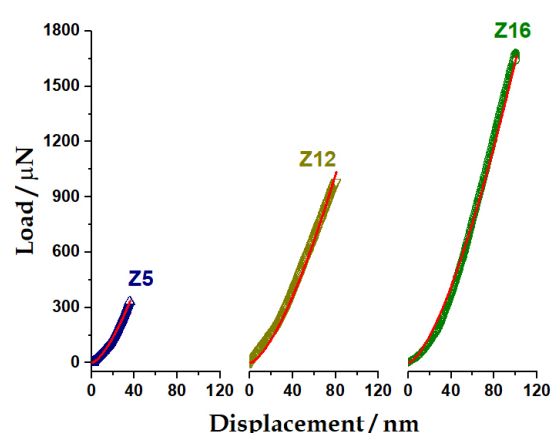


**Fig. 4.** (Color online) Load-depth curves for films using a 450  $\mu$ N load. Measured displacements were higher than 30 nm for every film.

**Table 2.** Thickness ( $t$ ), average elastic modulus ( $E_r$ ), hardness ( $H$ ) and wear volume (Wear) of films. The wear volume was obtained after 15 cycles under a 350  $\mu$ N load.

Film	$t$ / mm	$E_r$ / GPa	$H$ / GPa	Wear / $\mu\text{m}^3$	Reference
Z5	0.57	$96.7 \pm 11.5$	$4.5 \pm 0.4$	38.32	This work
Z12	1.25	$111.5 \pm 18.3$	$5.3 \pm 1.6$	53.68	This work
Z16	1.60	$100.0 \pm 21.5$	$5.9 \pm 2.2$	44.12	This work
ZnO	52.7	$108.2 \pm 7.3$	$7.3 \pm 0.8$	7.68	[23]
	50	$105.5 \pm 5.1$	$9.35 \pm 0.94$	--	[24]
	32	93	9.18	--	[3]

ionic substances and metals the bonding is delocalized, and extrinsic factors such as grain boundaries, precipitates and impurities, are used to determinate the hardness. FE-SEM images show a grain boundary variation with thickness increment. It can be suggested that the threading dislocations in an epitaxial layer under the indent region could be produced due grain boundaries strain compensation site [24]. When the nanoindenter gives a load on the films, these tightly linked grains will uniformly absorb and propagate the pressure produced by this load without threading dislocations because of arbitrary arrangement of the grain boundaries and return to nanoindenter with compressive stress. Such compressive stress can be larger than that of epitaxial layers presented by suddenly engendered threading dislocations [27].

Comparing other transparent oxides (Table 2), the films showed good stiffness and hardness. However, ZnO showed a relatively low mechanical performance compared to values reported by other researchers [3, 26]. The wear behavior observed is strongly related to the hardness behavior for each film, which is related to the wear volume. In this way, Z5 and Z16 showed lower values than Z12, suggesting that they protected the indentation point to a certain extent before the damage occurred.

The wear measurements were made over a  $20 \mu\text{m}^2$  area. Based on post-test Z-heights of  $20 \mu\text{m}$  nano wear areas, results with associated wear forces show no film failure. Nanowear results on samples can rank the best wear resistance analyzed film failure at each load. Using this ranking system, results in Table 2 show the ranking order for best wear resistance to be Z5, Z12, and Z16, which agrees with Scanning Probe Microscopy. Although these are promising results, further studies are needed before protective oxide coatings, e.g., ophthalmics, automotive or flat panel display industry are prepared by this spraying procedure.

In general, hard materials have high resistance to surface damage. Furthermore, Leyland et al. proposed that materials with a high hardness-to-Young's modulus ratio ( $H/E$ ) exhibit high wear resistance [28], which makes these films suitable for optoelectronic applications such as solar energy devices. In this work, the  $H/E$  ratio increases with increasing thickness, indicating that thicker films have higher wear resistance capacity. This increase is also due to the increase in hardness because of the incremental load. These films have relatively high  $H/E$  ratio values of  $0.047 - 0.06$  compared to works reported in the literature [25], where they report lower  $H/E$  ratios values for even thicker films. In other words, despite the low dimensionality of thin ZnO films, they have better mechanical properties compared to thicker films, demonstrating the benefits of the spray pyrolysis technique. However, when carrying out an analysis relating the hardness  $H$ , the elastic modulus  $E$ , and the radius of the indenter's contact sphere  $r$ , another parameter can be determined to indicate the tribological properties of the material, for example, the contact yield pressure  $P_y$ , which is given by the expression:

$$P_y = 0.78r^2 \left( \frac{H^3}{E^2} \right). \quad (6)$$

This parameter indicates the materials resistance to plastic deformation. According to Leyland [28], a high hardness

material typically has a yield pressure value of approximately three times the hardness value. For the films under study, the  $P_y$  values calculated for films Z5, Z12, and Z16 were 4.75, 5.83, and 10 GPa, respectively. In this way, it is established that thin zinc oxide films have low resistance to plastic deformation since the  $P_y/H$  ratio for each film is below 3 [28]. These values are shown in Table 3.

$H/E$  values reported in the literature seem to be higher than those shown in this work. For instance, a value of 0.07 was reported in [24], 0.09 in [27], and 0.1 in [3]. Thus, a relationship can be established between the  $H/E$  ratio and the thickness of the films, possibly due to the localized increased hardness  $H$  in the indented area of the film.

**Table 3.** Hardness ( $H$ ), contact yield pressure ( $P_y$ ), hardness-yield strength ratio ( $P_y/H$ ) and hardness-Young's modulus ratio ( $H/E$ ).

Film	$H / \text{GPa}$	$P_y / \text{GPa}$	$P_y/H$	$H/E$
Z5	$4.5 \pm 0.4$	4.75	1.05	$0.047 \pm 0.003$
Z12	$5.3 \pm 1.6$	5.83	1.10	$0.048 \pm 0.008$
Z16	$5.9 \pm 2.2$	10	1.69	$0.060 \pm 0.01$

#### 4. Conclusions

An extensive study of the mechanical properties of thin films based on ZnO grown by spray-pyrolysis was presented. The morphology of microstructures seen in the FE-SEM images shows a difference in the porosity of samples due to the increased size and grain shape. A relationship between film thickness and hardness was found. It was found that this relationship is attributed to the increase in the density of the film in the indented area, leading to a local increase in the thin film hardness. As the film thickness increases, the localized hardness also shows an increase, which can be attributed to the fact that the measuring equipment applies more force to adhere to the rule of 10% of the depth of the indentation with respect to the film thickness. Variations in hardness are due to the film density around the indentation point produced by the increase in the supplied charge. The obtained hardness values are in good agreement with those reported for this material and hard coatings. The result that the  $H/E$  ratio increases with the thickness of the films is consistent with previous theories and studies in this field, and has important implications for the design and optimization of the mechanical properties of thin films. The latter is also linked to the optical and electrical properties of films. The results obtained show that the thin films based on ZnO studied in this work can be used for optoelectronic devices according to the Mohs scale, where 1 corresponds to talc and 10 to diamond. In this case, the Mohs index places ZnO films above 4.

**Author contributions.** E. A. Villegas: Investigation, Methodology, Writing. R. Parra: Conceptualization, Methodology, Supervision, Reviewing and editing, Funding acquisition. L. A. Ramajo: Conceptualization, Methodology, Supervision, Writing, Funding acquisition.

**Research Data Policy and Data Availability Statements.** The datasets analyzed during the present study are available from the corresponding author on request.

*Declaration of competing interest.* The authors declare that they have no known competing financial interests or personal relationships that could have appeared to influence the work reported in this paper.

*Acknowledgements.* The authors gratefully acknowledge the support of the CONICET (PIP2487) , UNMdP (15 / G577) and ANICYT (PICT Start up 2021-26).

## References

1. E.A. Villegas, C.M. Aldao, R. Savu, L.A. Ramajo, R. Parra. Phys. status solidi. 215 (11), 1800107 (2018). [Crossref](#)
2. E.A. Villegas, L.A. Ramajo, M.E. Lere, M.S. Castro, R. Parra. Mater. Sci. Semicond. Process. 121, 105412 (2021). [Crossref](#)
3. S. Zhao et al. J. Alloys Compd. 319 (4), 126 (2017).
4. G. Zheng et al. Mater. Sci. Semicond. Process. 112, 105016 (2020). [Crossref](#)
5. O. Çiçek, S. Kurnaz, A. Bekar, Ö. Öztürk. Compos. Part B Eng. 174, 106987 (2019). [Crossref](#)
6. D. Staub, S. Meille, V. Le Corre, L. Rouleau, J. Chevalier. Acta Mater. 107, 261 (2016). [Crossref](#)
7. K. von Fieandt et al. Thin Solid Films. 693, 137685 (2020) [Crossref](#)
8. C. Yang, J.R. Qu, Z.Y. Wu. Sol. Energy. 214, 542 (2021). [Crossref](#) <https://doi.org/10.1016/j.solener.2020.12.014>
9. G.B. Lee, S.H. Song, M.W. Lee, Y.J. Kim, B.H. Choi. Appl. Surf. Sci. 535, 147731 (2021). [Crossref](#)
10. C.Y. Yen et al. Appl. Surf. Sci. 257 (17), 7900 (2011). [Crossref](#)
11. R. Siddheswaran et al. J. Alloys Compd. 636, 85 (2015). [Crossref](#)
12. R.G. Gordon. MRS Bull. 25 (8), 52 (2000). [Crossref](#)
13. M. Zhang, Y.P. Zheng, A.F.T. Mak. Med. Eng. Phys. 19 (6), 512 (1997). [Crossref](#)
14. S.Y. Chang, Y.C. Hsiao, Y.C. Huang. Surf. Coatings Technol. 202 (22 – 23), 5416 (2008). [Crossref](#)
15. R.J. Hong, X. Jiang, B. Szyszka, V. Sittinger, A. Pflug. Appl. Surf. Sci. 207 (1–4), 341 (2003). [Crossref](#)
16. U.S. Mbamara, B. Olofinjana, O.O. Ajayi, C. Lorenzo-Martin, E.I. Obiajunwa, E.O.B. Ajayi. Eng. Sci. Technol. an Int. J. 19 (2), 956 (2016). [Crossref](#)
17. A. Osaka, S. Takao, K. Oda, J. Takada, Y. Miura. Mem. Fac. Eng. Okayama Univ. 24 (1), 53 (1989).
18. G. Turgut et al. J. Mater. Sci. Mater. Electron. 25 (6), 2808 (2014). [Crossref](#)
19. M.A. Ramírez, R. Parra, M.M. Reboreda, J.A. Varela, M.S. Castro, L. Ramajo. Mater. Lett. 64 (10), 1226 (2010). [Crossref](#)
20. W.C. Oliver, G.M. Pharr. J. Mater. Res. 7 (6), 1564 (1992). [Crossref](#)
21. W.C. Oliver, G.M. Pharr. J. Mater. Res. 19 (1), 3 (2004). [Crossref](#)
22. N. Winkler, R.A. Wibowo, W. Kautek, T. Dimopoulos. J. Mater. Chem. C. 7, 3889 (2019). [Crossref](#)
23. E.A. Villegas, R. Parra, L. Ramajo. J. Mater. Sci. Mater. Electron. 30 (2), 1360 (2019). [Crossref](#)
24. S. Higashino et al. Surf. Coatings Technol. 325 (1–2), 346 (2017). [Crossref](#)
25. V.A. Coleman et al. Appl. Phys. Lett. 86 (20), 203105 (2005). [Crossref](#)
26. Z. Chen, X. Wang, N. Brandon, A. Atkinson. J. Eur. Ceram. Soc. 37 (3), 1031 (2017). [Crossref](#)
27. S. Zhao et al. Appl. Surf. Sci. 253 (2), 726 (2006). [Crossref](#)
28. A. Leyland, A. Matthews. Wear. 246 (1–2), 1–11 (2000). [Crossref](#)